Progress In Electromagnetics Research Letters, Vol. 100, 99–107, 2021

A Compact Dual-Band Wideband Circularly Polarized Microstrip Antenna for Sub-6G Application

Zhong Yu, Leiyan Huang*, Qi Gao, and Bingwen He

Abstract—A dual-band wideband circularly polarized (CP) microstrip antenna is proposed for sub-6G application. The antenna consists of an upper L-shaped radiator and two circular strips on the ground. This produces the right-handed circular polarization (RHCP) in the Wi-Fi (2.4–2.48 GHz) and n77 (3.3-4.2 GHz) band with the help of two circular strips at the left and right corners on the lower ground. The antenna occupies a small radiating area of $45 \times 45 \times 1.0\,\text{mm}^3$. The measured results show wide -10 dB reflection coefficient bandwidths of 46.4% (1.82–2.92 GHz) and 40.5% (3.15–4.75 GHz). The 3-dB axial ratio bandwidths of the antenna are 25.1% (1.88–2.42 GHz) and 40.6% (3.20–4.83 GHz). The measured peak gains are 4.8 and 7.5 dBi at the lower and higher bands, respectively. Therefore, the proposed antenna in this study is suitable for the dual-band wideband CP antenna as a reference.

1. INTRODUCTION

Circular polarization (CP) of radio waves has special advantages in communication application. For example, CP antenna avoids polarization mismatch and improves communications capacity and quality [1, 2]. Since various modern wireless communication systems require wideband and high-speed information processing capabilities, antennas are also required to have wideband or multi-band operating characteristics. Besides, the demand for microstrip antennas with small size and high gain operating frequencies is increasing [3]. CP is an ideal characteristic of wideband antennas. In view of this, compact wideband multi-frequency antennas with CP characteristics have become a research hotspot in the industry [4, 5].

In recent years, many scholars have done a lot of researches on dual-band CP microstrip antennas. In [6], a dual-band single-feed CP microstrip antenna is composed of two layers of microstrip metal patches. The CP radiation is realized by adjusting the position of feed points and its CP radiation at 3.5 and 5.18 GHz. The antenna is designed to realize dual-band CP radiation by placing the rectangular ring antenna at the first and second layers, respectively, and the thickness of the antenna is 20 mm [7]. In [8], the mentioned antenna achieves dual-band CP radiation by cutting two circular slots in a noncentral structure, and the antenna works at 2.1 and 3.6 GHz with 3-dB AR bandwidths (ARBW) of 9 and 21 MHz. The proposed single-feed dual-band CP designs are achieved by inserting four Y-shaped slits at the patch corners of a square microstrip antenna [9]. In [10], dual-band CP characteristic is achieved by combining the slot mode working in the GPS L1 band and the patch mode operating in the GPS L2 band. In [11], lower band right-handed circular polarization (RHCP) is mainly realized by the inverted L-shaped strip (ILSS), and the upper band left-handed circularly polarized (LHCP) is mainly achieved by the offset feed structure (OFS). The designed antenna is based on a single-layer and single-feed configuration [12]. However, in the case of low profile and compact size, it is rare for CP microstrip antennas to achieve both impedance and AR wideband in both operating bands.

Received 27 August 2021, Accepted 1 October 2021, Scheduled 10 October 2021

* Corresponding author: Leiyan Huang (hly814@stu.xupt.edu.cn).

The authors are with the School of Communication and Information Engineering, Xi'an University of Posts & Telecommunications, Xi'an, China.

In this paper, a novel embedded circular strips method is proposed for dual-band wideband CP microstrip antenna applications. At the same time, the designed antenna uses a non-centered L-shaped radiator to generate the lower and higher bands instead of the traditional central feeding mode. By adding two circular strips at the left and right corners on the lower ground, the 3-dB ARBWs of the antenna and 25.1% and 40.6% at the lower and higher bands, respectively.

2. ANTENNA CONFIGURATION

2.1. Antenna Model

Figure 1 shows the proposed antenna model. The antenna consists of an upper L-shaped radiator and a lower ground. The antenna is designed on an FR-4 substrate (with relative permittivity of 4.4 and loss tangent of 0.02) of size $45 \times 45 \times 1.0\,\text{mm}^3$. Unlike the rectangular strip proposed in [13], the upper non-central L-shaped radiator is fed by a $50\,\Omega$ microstrip line ($L_f \times W_f$). Two embedded circular strips (R_2, R_3) are added to the left and right corners of the ground. The simulation software ANSYS HFSS 15.0 is used to optimize and analyze the antenna parameters. The final designed CP antenna size is obtained, as shown in Table 1.

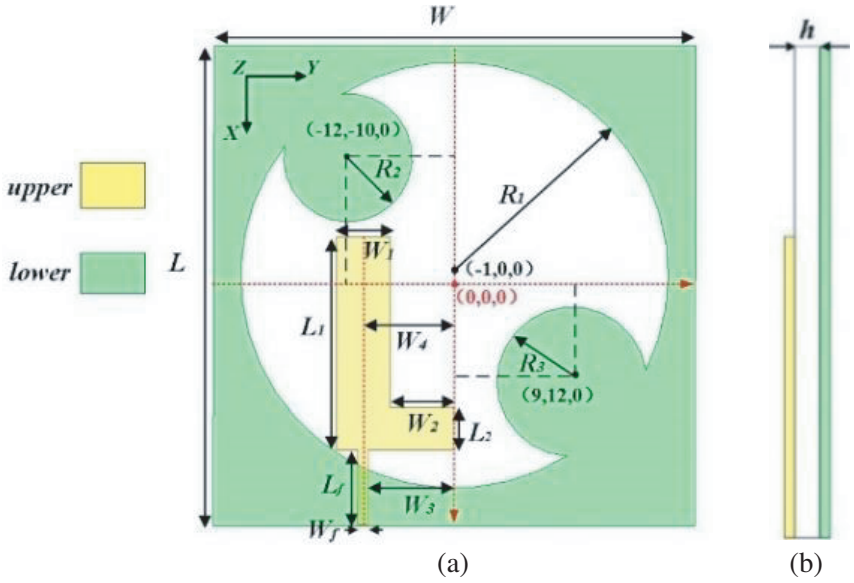

Figure 1. Structure layout of the proposed antenna: (a) Top view; (b) Side view.

Table 1. The dimensions of the proposed antenna.

Parameter	Value (mm)	Parameter	Value (mm)	Parameter	Value (mm)	Parameter	Value (mm)
L	45	W_1	5	L_f	7	R_1	20
W	45	W_2	6	W_f	1	R_2	6
L_1	20	W_3	8	h	1	R_3	7
L_2	4	W_4	8.5				

2.2. Antenna Analysis

The design procedure of the dual-band wideband CP antenna structure is presented in Figure 2. As displayed in Figure 2(a) (Step-1), a wide circular slot is etched from the square-shaped patch, which is

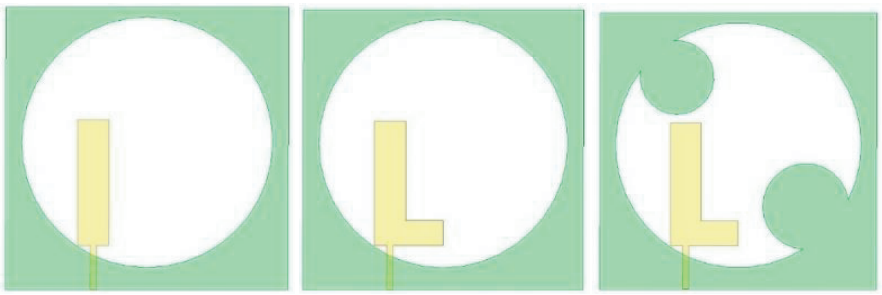

(a) (b) (c)

Figure 2. Evolution of dual-band wideband CP antenna: (a) Step-1; (b) Step-2; (c) Step-3.

fed by a non-center positioned microstrip feed line. Then, an L-shaped radiator is formed by adding another rectangular radiator, as illustrated in Figure 2(b) (Step-2). Figure 2(c) (Step-3) shows that two circular strips (R_2, R_3) are bulged towards the center of the etched slot.

The reflection coefficient (S_{11}) and axial ratio of the antenna for each step are given in Figures 3(a) and (b). The antenna exhibits the simulated impedance bandwidths of 50.1% (1.75–2.92 GHz) and 42.4% (3.12–4.80 GHz). The simulated 3-dB ARBWs are 33.3% (1.80–2.52 GHz) and 45.6% (3.05–4.85 GHz). The antenna of Step-1 exhibits linear polarization (LP) characteristics, and the S_{11} performance is bad almost within the whole bandwidth. After an L-shaped radiator is formed, the lower ARBW of Step-2 is improved. The S_{11} performance and ARBW of Step-3 have been greatly improved by adding two circular strips at the left and right corners on the lower ground. The proposed antenna achieves wideband CP characteristics in the lower and higher bands, respectively.

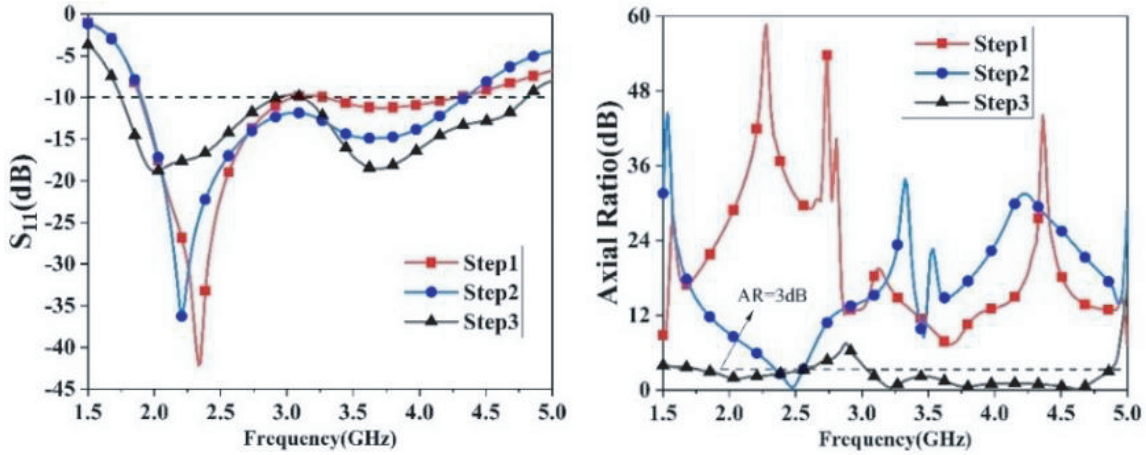

(a) (b)

Figure 3. Comparison of the antenna design steps: (a) Reflection coefficient; (b) Axial ratio.

Figure 2(a) (Step-1) of the antenna is a conventional printed line-polarized antenna that has only one rectangular radiator ($L_1 \times W_1$). It can be seen from Figure 3(a) that the resonant path ($L_f + L_1$) is about one quarter of the medium wavelength, so the lowest resonant frequency of the Step-1 antenna is about 2.4 GHz. To enable the antenna to operate at high frequency bands, another rectangular radiator ($L_2 \times W_2$) is added to the beginning of the rectangular radiator ($L_1 \times W_1$). At the same time, the non-central position of the radiator breaks the symmetry of LP and achieves the circular polarization effect of low frequency, but the ARBW is very narrow. To achieve the characteristics of high frequency circular polarization and broaden the ARBW, circular matching strips (R_2, R_3) are used. Two circular

strips added to the ground and an asymmetric feed structure provide a 90° phase difference to achieve the high frequency circular polarization characteristics of the antenna. Adjusting the dimensions and center position of the two circular strips on the ground can improve the impedance matching and broaden bandwidth of the antenna [14, 15].

2.3. Parameter Study

In order to obtain the optimal antenna dimensions, parameters of the two circular strips (R_2, R_3) on the antenna ground are compared and analyzed, as shown in Figure 4. It can be seen from Figure 4(a) that R_2 and R_3 are the key parameters affecting the antenna impedance matching. Figure 4(b) shows the change of ARBW with R_2 and R_3. Changes in R_2 and R_3 affect the surface current amplitudes of the two circular stripes. The adjustment of the current amplitude of each structure results in the change of superposition current direction at different phases. Therefore, the high-frequency ARBW becomes narrower.

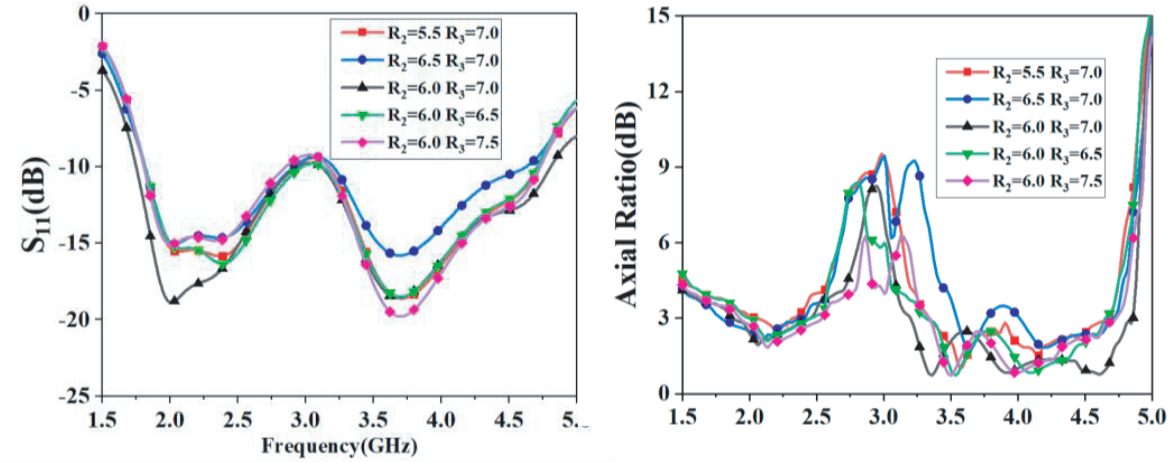

Figure 4. Influence of R_2 and R_3 on antenna performance: (a) Reflection coefficient; (b) Axial ratio.

2.4. Surface Current Distributions

The surface current distribution of the proposed antenna is studied to explain the dual-band wideband CP mechanism. Figure 5 shows the surface current distribution of the antenna at 2.0 GHz and 3.6 GHz.

As shown in Figure 5(a), the surface current ($J = 0°$) at the $\omega t = 0$ phase is mainly formed by the surface currents on the L-shaped radiator (J_8 and J_9) and the lower ground (J_1, J_2, J_3, J_4, J_5, J_6, and J_7). Obviously, the superposition current in the $-x$ direction ($J_1 + J_2$) is stronger than the superposition current in the $+x$ direction ($J_5 + J_6$), and the superposition current in the $-y$ direction ($J_3 + J_4$) is stronger than the superposition current in the $+y$ direction ($J_7 + J_8$). Thus, the amplitude of superimposed $J = 0°$ current is mainly controlled by the L-shaped radiator and the square-shaped ground with wide circular slot. After the currents in opposite directions cancel each other, the vector of the $J = 0°$ superimposed current goes along the $-x$ axis direction with φ about 45°. For the superimposed surface current distribution at the $\omega t = T/4$ ($J = 90°$) phase, the current distribution is also mainly produced by the surface currents on the L-shaped radiator (J_8 andJ_9) and the lower ground (J_1, J_2, J_3, J_4, J_5, J_6, and J_7). Actually, the superposition current in the $+x$ direction ($J_1 + J_2 + J_3$) is stronger than the superposition current in the $-x$ direction (J_8), and the superposition current in the $-y$ direction($J_4 + J_5 + J_6 + J_7$) is stronger than the superposition current in the $+y$ direction (J_9). Thus, the amplitude of superimposed $J = 90°$ current is mainly controlled by the two circular strips added to the lower ground. After the currents in opposite directions cancel each other, the vector of the $J = 90°$ superimposed current goes along the $-x$ axis direction with φ about 135°. Therefore, the

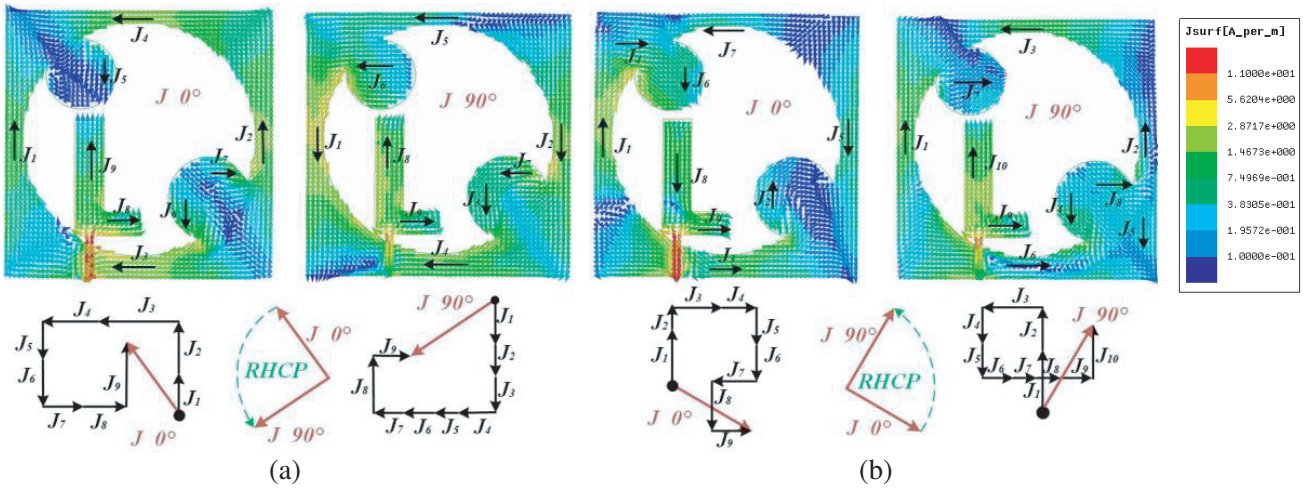

Figure 5. Simulated surface current distributions: (a) 2.0 GHz; (b) 3.6 GHz.

dominant current vector in antenna rotates counterclockwise, hence validating the RHCP operation, in the $+z$ direction at 2.0 GHz.

Similarly, in Figure 5(b), the surface current ($J = 0°$) at the $\omega t = 0$ phase is mainly formed by the surface currents on the L-shaped radiator (J_8 and J_9) and the circular strip added to the left side of the ground (J_4 and J_6). The surface currents on lower ground (J_1, J_2, J_3, J_5 and J_7) cancel each other. After the currents in opposite directions cancel each other, the vector of the $J = 0°$ superimposed current goes along the $+x$ axis direction with φ about 45°. Besides, the surface current ($J = 90°$) at the $\omega t = 0$ phase is mainly formed by the surface currents on the L-shaped radiator (J_9 and J_{10}) and the circular strip added to the right side of the ground (J_8). The surface currents on lower ground (J_1, J_2, J_3, J_4, J_5, J_6, and J_7) cancel each other. After the currents in opposite directions cancel each other, the vector of the $J = 90°$ superimposed current goes along the $+x$ axis direction with φ about 135°. Similarly, in Figure 5(b), the dominant current vector in antenna rotates counterclockwise, hence validating the RHCP operation, in the $+z$ direction at 3.6 GHz.

3. RESULTS AND DISCUSSION

According to the optimized size, the dual-band wideband CP antenna system has been successfully fabricated and measured. The proposed antenna prototype (top and bottom view) is presented in Figure 6(a). The S-parameters of the antenna were measured using the Agilent E5071C Network

Figure 6. Proposed CP antenna: (a) Prototype; (b) The far field measurement.

Analyzer. Besides, the far field measurement setup inside a Satimo-SG64 Anechoic Chamber system is shown in Figure 6(b).

Figure 7 shows the simulated and measured S_{11} of the antenna varied with frequency. It can be seen that the -10 dB impedance bandwidths of the antenna are 46.4% (1.82–2.92 GHz) and 40.5% (3.15–4.75 GHz). However, the antenna has frequency deviation in the lower frequency, which may be caused by dimensional deviation of the antenna model.

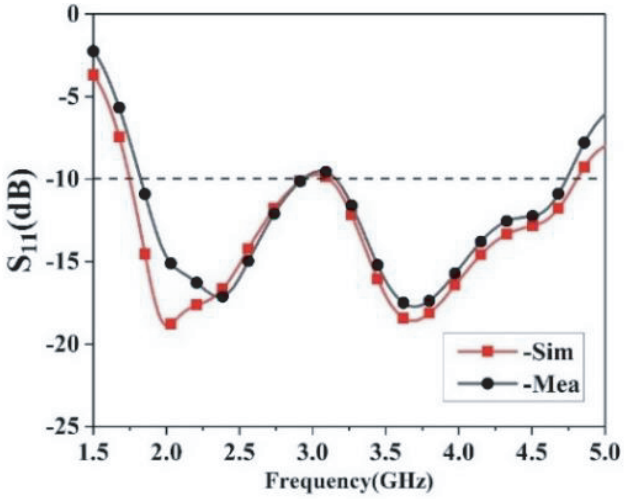

Figure 7. S_{11} result of the proposed CP antenna.

It is observed from Figure 8(a) that a good quality of circular polarization is achieved in the band of interest. The measured antenna ARBWs are 25.1% (1.88–2.42 GHz) and 40.6% (3.20–4.83 GHz). Figure 8(b) shows that the measured antenna peak gains are 4.8 dBi at 2.5 GHz and 7.5 dBi at 4.0 GHz, respectively. This shows that adding two circular strips at the left and right corners on the lower ground greatly improves the axial ratio characteristics of the proposed antenna.

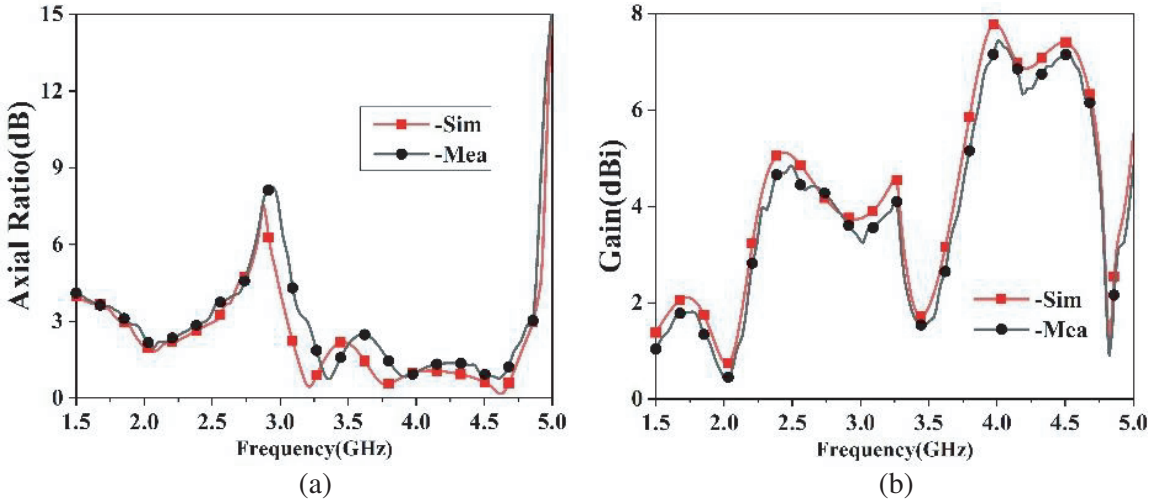

Figure 8. Simulated and measured of the proposed CP MIMO antenna: (a) Axial ratio; (b) Gain.

Figure 9 shows the 2D radiation pattern of the CP antenna at 2.0 GHz and 3.6 GHz in xz-plane and yz-plane. It can be seen from Figure 9(a) that the main polarization of the antenna radiated at 2.0 GHz is an RHCP wave in the $+z$ direction. The difference between the RHCP wave and LHC) wave

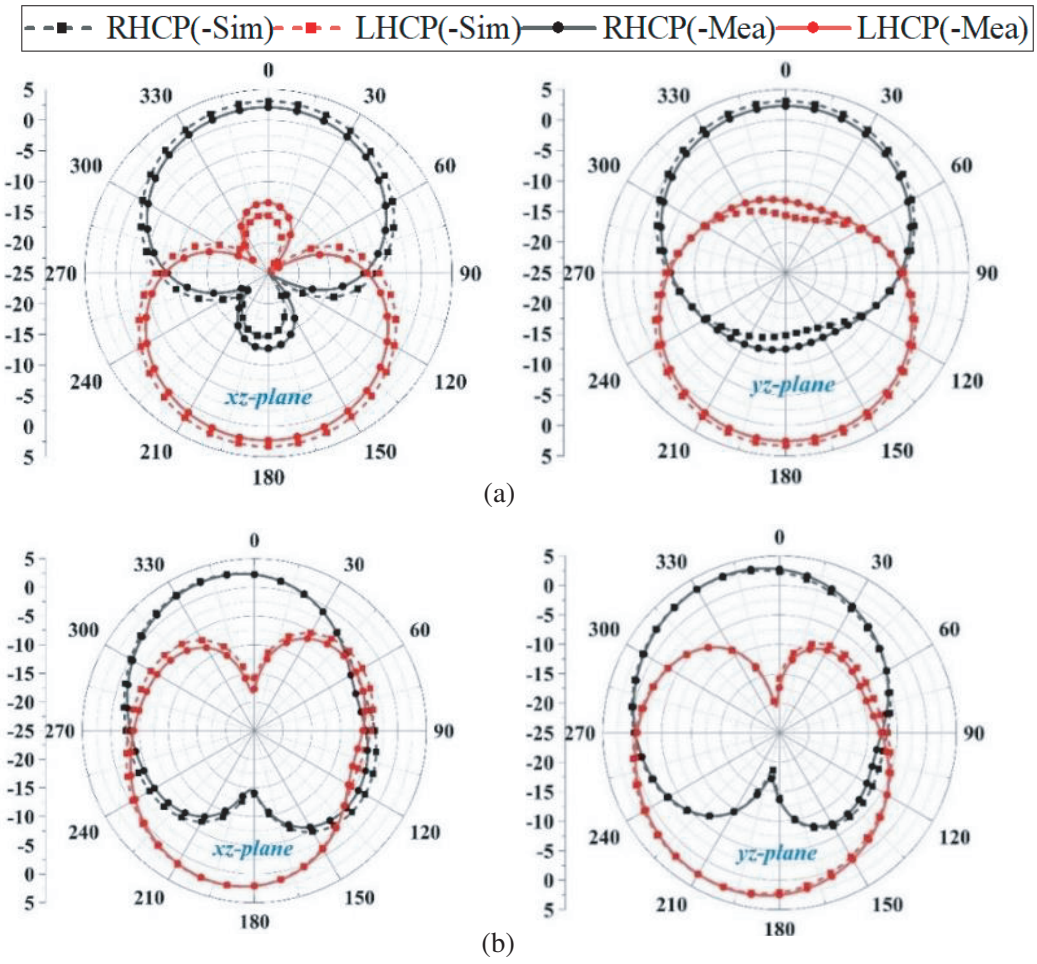

Figure 9. 2-D radiation patterns of the CP antenna. (a) 2.0 GHz. (b) 3.6 GHz.

of the antenna tested in the $+z$ direction is about 15.6 dB. Similarly, Figure 9(b) shows that the main polarization of the antenna radiated at 3.6 GHz is an RHCP wave in the $+z$ direction. The difference between the RHCP wave and LHCP wave tested by the antenna in the $+z$ direction is about 19.7 dB. The measured and simulated radiation patterns are basically the same.

Compared with other studies on dual-band CP antennas as in Table 2 [9–12], the proposed antenna system has certain advantages over other studies in not only bandwidth but also antenna size. The two circular strips at the left and right corners on the lower ground greatly expand the impedance bandwidth

Table 2. Performance comparison between the proposed antenna and previous work.

Work	Total Size (mm^3)	Impedance bandwidth (GHz)		3 dB AR bandwidth (GHz)		Peak Gain (dBi)
		Lower band	Higher band	Lower band	Higher band	
[9]	$75 \times 75 \times 1.6$	1.61–1.64	2.85–2.92	1.62–1.64	2.86–2.89	4, 1.2
[10]	$80 \times 80 \times 30$	1.12–1.69		1.18–1.26	1.49–1.61	7.72, 8.11
[11]	$50 \times 50 \times 1.0$	1.82–6.36		1.91–3.36	4.47–6.41	4.2, 3.4
[12]	$50 \times 50 \times 1.6$	1.83–3.23	4.99–6.16	1.88–2.60	4.95–6.80	3.36, 4.19
Prop.	**$45 \times 45 \times 10$**	**1.82–2.92**	**3.15–4.75**	**1.88–2.42**	**3.20–4.83**	**4.8, 7.5**

and ARBW of the antennas. Apparently, the proposed antenna also has high peak gain at the higher band. Therefore, the proposed antenna in this study is suitable for the dual-band wideband CP antenna as a reference.

4. CONCLUSION

This paper proposes a compact dual-band wideband CP microstrip antenna for Sub-6G application. The dual-frequency radiation of the antenna is realized through a non-centered L-shaped radiator. The characteristic of dual-band wideband CP is achieved by adding two circular strips at the left and right corners on the lower ground. The −10 dB impedance bandwidths are 46.4% and 40.5%. Meanwhile, the measured antenna 3-dB ARBWs are 25.1% and 40.6%. Consequently, the proposed antenna has good application value for Sub-6G.

REFERENCES

1. Dicandia, F. A., S. Genovesi, and A. Monorchio, "Analysis of the performance enhancement of MIMO systems employing circular polarization," *IEEE Transactions on Antennas and Propagation*, Vol. 65, No. 9, 4824–4835, Sep. 2017.
2. Rajanna, P. K. T., K. Rudramuni, and K. Kandasamy, "A wideband circularly polarized slot antenna backed by a frequency selective surface,", *Journal of Electromagnetic Engineering and Science*, Vol. 19, No. 3, 166–171, Jul. 2019 (in English).
3. Liang, J., C. C. Chiau, X. Chen, and C. G. Parini, "Study of a printed circular disc monopole antenna for UWB systems," *IEEE Transactions on Antennas and Propagation*, Vol. 53, No. 11, 3500–3504, 2005.
4. Huang, Y. J., L. Yang, J. Li, Y. Wang, and G. J. Wen, "Polarization conversion of metasurface for the application of wide band low-profile circular polarization slot antenna," *Applied Physics Letters*, Vol. 109, No. 5, Art. No. 054101, Aug. 2016.
5. Jan, J., C. Pan, K. Chiu, and H. Chen, "Broadband CPW-fed circularly-polarized slot antenna with an open slot," *IEEE Transactions on Antennas and Propagation*, Vol. 61, No. 3, 1418–1422, 2013.
6. Qian, K. and X. Tang, "Compact LTCC dual-band circularly polarized perturbed hexagonal microstrip antenna," *IEEE Antennas and Wireless Propagation Letters*, Vol. 10, 1212–1215, 2011.
7. Li, Y., B. Tian, J. Xue, and G. Ge, "Compact dual-band circularly polarized antenna design for navigation terminals," *IEEE Antennas and Wireless Propagation Letters*, Vol. 15, 802–805, 2016.
8. Liang, Z., D. Yang, X. Wei, and E. Li, "Dual-band dual circularly polarized microstrip antenna with two eccentric rings and an arc-shaped conducting strip," *IEEE Antennas and Wireless Propagation Letters*, Vol. 15, 834–837, 2016.
9. Y. Kai-Ping and W. Kin-Lu, "Dual-band circularly-polarized square microstrip antenna," *IEEE Transactions on Antennas and Propagation*, Vol. 49, No. 3, 377–382, 2001.
10. Lee, S., Y. Yang, K. Y. Lee, and K. C. Hwang, "Dual-band circularly polarized annular slot antenna with a lumped inductor for GPS application," *IEEE Transactions on Antennas and Propagation*, Vol. 68, No. 12, 8197–8202, Dec. 2020.
11. Xu, R., J. Y. Li, J. Liu, S. G. Zhou, K. Wei, and Z. J. Xing, "A simple design of compact dual-wideband square slot antenna with dual-sense circularly polarized radiation for WLAN/Wi-Fi communications," *IEEE Transactions on Antennas and Propagation*, Vol. 66, No. 9, 4884–4889, Sep. 2018.
12. Weng, W. C., J. Y. Sze, and C. F. Chen, "A dual-broadband circularly polarized slot antenna for WLAN applications," *IEEE Transactions on Antennas and Propagation*, Vol. 62, No. 5, 2837–2841, May 2014.
13. Xu, R., J.-Y. Li, Y.-X. Qi, G.-W. Yang, and J.-J. Yang, "A design of triple-wideband triple-sense circularly polarized square slot antenna," *IEEE Antennas and Wireless Propagation Letters*, Vol. 16, 1763–1766, 2017.

14. Mason Moore, Z. I. and S. Lim, "A size-reduced, broadband, bidirectional, circularly polarized antenna for potential application in WLAN, WiMAX, 4G, and 5G frequency bands," *Progress In Electromagnetics Research C*, Vol. 114, 1–11, 2021.
15. Sung, Y., "Bandwidth enhancement of a microstrip line-fed printed wide-slot antenna with a parasitic center patch," *IEEE Transactions on Antennas and Propagation*, Vol. 60, No. 4, 1712–1716, 2012.